Composites Part B 143 (2018) 36–46

Contents lists available at ScienceDirect

Composites Part B

journal homepage: www.elsevier.com/locate/compositesb

Ultra-high-speed processing of nanomaterial-reinforced woven carbon fiber/polyamide 6 composites using reactive thermoplastic resin transfer molding

Byeong-Joo Kim, Sang-Hyup Cha, Young-Bin Park*

Department of Mechanical and Aerospace Engineering, Ulsan National Institute of Science and Technology (UNIST), UNIST-gil 50, Ulju-gun, Ulsan 44919, Republic of Korea

ARTICLE INFO

Keywords:
Carbon fibres
Thermoplastic resin
Mechanical properties
Resin transfer molding

ABSTRACT

High-speed molding of continuous carbon fiber-reinforced composites was carried out by thermoplastic resin transfer molding using a very-low-viscosity thermoplastic monomer. After dispersing 0.1 wt.% of various nanomaterials in ε-caprolactam, a monomer of anionic polymerized polyamide 6 (A-PA6), the processing temperature and catalyst-activator contents were optimized based on the polymerization induction time required for resin injection in the mold. Additionally, the dispersion stability, solidification time, monomer conversion, crystallinity and mechanical properties of the composites were evaluated. Higher dispersion stability of the nanomaterials in A-PA6 resulted in a significantly shortened process cycle time – on the order of seconds –and higher crystallinity in the composite. In addition, carbon fibers treated with atmospheric plasma were used to increase the rate of resin impregnation into fibers. These factors not only increased composite fabrication productivity but also enhanced its mechanical properties.

1. Introduction

In recent years, legislation to regulate automobile fuel consumption and emissions have been strengthened in developed countries. Therefore, lightweight fiber-reinforced composites have attracted much interest from the automobile industry. In particular, efforts are underway to apply long fiber-reinforced thermoplastic to seatback frames and battery storage for hybrid vehicles [1]. However, further improvement of the physical properties of these composites is necessary to meet the future demand for lighter weighing composites, and thus, continuous fiber-reinforced thermoplastics is necessary.

Despite the fact that thermoplastic composites have many advantageous properties such as high impact resistance [2] and recyclability [3], they cannot be produced effectively along with the continuous fibers because of the difficulty associated with impregnating high-viscosity molten resin into continuous fiber textile. Reaction injection molding is a widely practiced processing method for fiber-reinforced thermoset composites; however, a similar concept for thermoplastics, known as thermoplastic resin transfer molding (T-RTM), has only recently been developed [4–8]. Anionic ring-opening polymerization of ε-caprolactam (CPL) occurs much faster than the hydrolytic reaction [9]; therefore, it is most suitable for the T-RTM process. The CPL, a precursor to anionic polymerized polyamide 6 (A-PA6), is injected in the low-viscosity monomer state into a mold charged with a fiber textile preform. Upon injection, the monomer reacts immediately with the pre-mixed catalyst and activator, leading to simultaneous polymerization and crystallization below the polymer melting and crystallization point. The viscosity of the resin used in T-RTM is 100 times lower than that required for the reaction processing of thermoset resins, and in particular, 160,000 times lower than that needed for the melting process of engineering thermoplastics [10]. Therefore, the T-RTM process not only has few product shape limitations, but is also very advantageous for resin impregnation into fibers and fast production.

For accelerating the reaction rate, it is typical to increase the catalyst-activator contents, or increase the polymerization temperature. An inert environment also increases the reaction rate, because oxygen and moisture in air deactivate the anions and active sites, as previously reported [11,12]. The increasing polymerization temperature increases the activation energy required for polymerization, inducing rapid reaction, but it decreases the polymer crystallinity and mechanical properties [5,13,14]. However, low polymerization temperature not only decreases the polymerization rate but also increases the crystallization rate, which induces reactive groups to be trapped inside the growing crystals before they are polymerized, thus causing low monomer conversion [5].

An improvement in resin impregnation through the surface treatment of fibers can also reduce the manufacturing process time. Instead of conventional surface treatment methods, which have a long

* Corresponding author.
E-mail address: ypark@unist.ac.kr (Y.-B. Park).

https://doi.org/10.1016/j.compositesb.2018.02.002
Received 19 December 2017; Received in revised form 27 December 2017; Accepted 1 February 2018

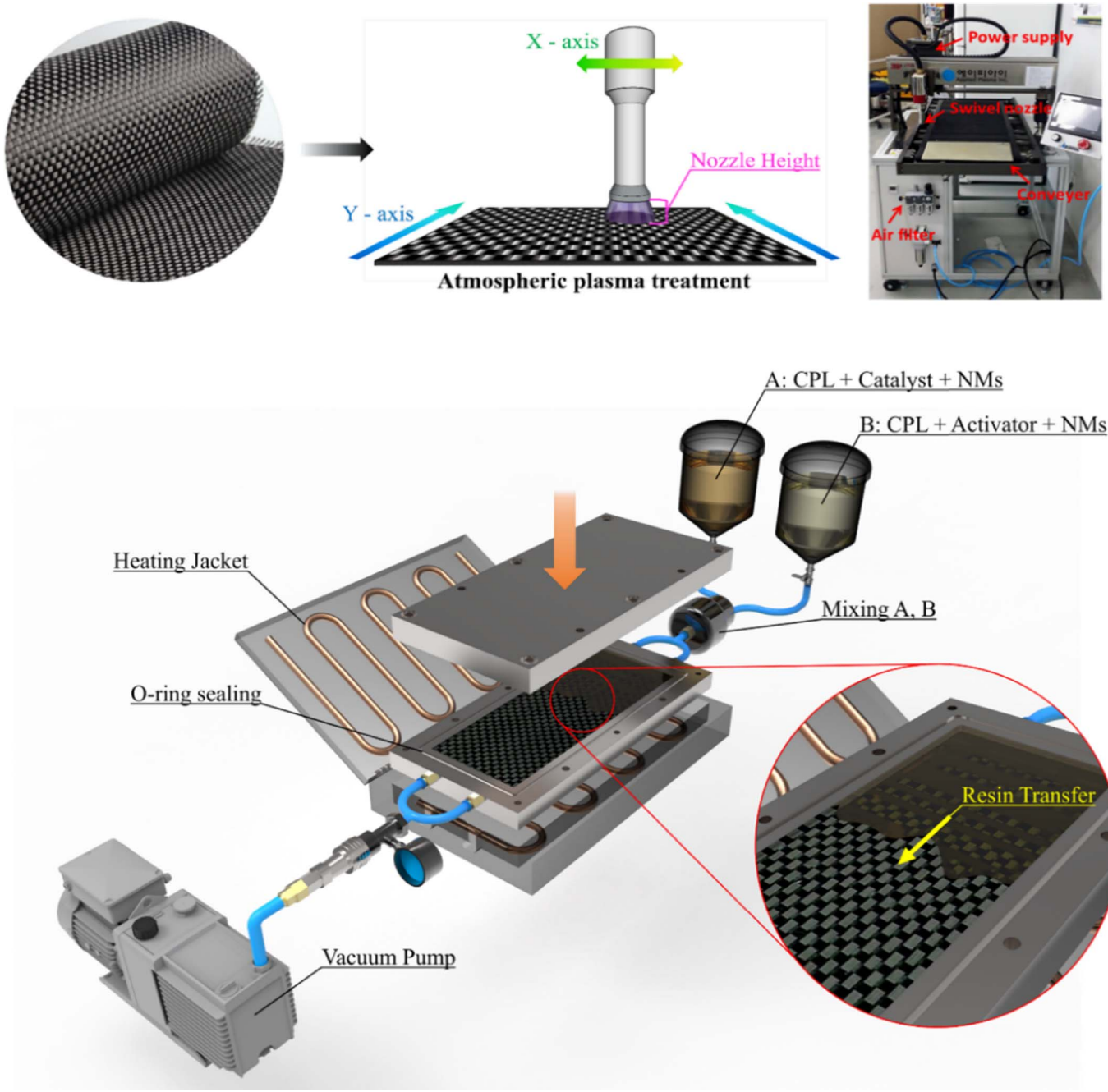

Fig. 1. Processing schematics of atmospheric plasma system and T-RTM.

treatment time and a limited sample size, atmospheric plasma treatment has recently shown many advantages such as continuous in-line processing capability and no vacuum chamber. Also, it can increase the polar functional groups [15–18] and roughness on the fiber surface, thereby making the fiber surface hydrophilic [19–21]. These factors result in an increased resin impregnation rate.

Nanomaterials (NMs) and fine particles have been applied as additives in various research fields, and they have especially used in polymer research field owing to their excellent properties as reinforcing agents [22–28]. In particular, NMs act as nucleating agents to promote the nucleation of crystallites within the polymer [29–32], thereby increasing the crystallization temperature and melting temperature [33,34]. These factors lead to the stabilization of the crystal structure [35], reduction in the crystal size [36], and increase in crystallinity as well as enhancement of the mechanical properties [22,24,36–39]. Furthermore, they increase the crystallization rate, which can improve the productivity and decreasing product shrinkage and distortion [40–43].

Fast polymerization and low viscosity are necessary for the T-RTM. Therefore, plain woven carbon fiber (WCF)-reinforced composites were developed using various NMs and plasma treatment to reduce the process cycle time without deteriorating the crystallinity and mechanical properties. The fabrication process parameters of NM/A-PA6/WCF composites were optimized with respect to polymerization induction time – which is the initial slow stage of a chemical reaction, after which the reaction accelerates and therefore governs the overall processing time – and dispersion stability, crystallinity and mechanical properties were investigated.

2. Experimental

2.1. Materials

Polyacrylonitrile-based plain WCFs (T-300, Toray Corporation, Japan) were used in this study. ε-Caprolactam (C2204, Sigma-Aldrich, USA), which has a low moisture content (< 100 ppm) and a low melting point (68 °C), was used as a precursor of A-PA6. Because sodium-based catalysts provide very short polymerization induction times as compared to magnesium-bromide-salt-based catalysts, which delay the onset of polymerization by several tens of minutes, a sodium-based catalyst (Addonyl® Kat_NL, Rhein Chemie, Germany) was used. Addonyl® 8120, an activator containing the blocked 1,6-hexamethylene diisocyanate, was used along with the catalyst. Various as-received NMs, including multiwalled carbon nanotube (MWCNT, CM-250, Hanwha Chemical, Korea), reduced graphene oxide (rGO, V30-100), graphene oxide (GO, V30, Standard Graphene, Korea), nanoclay (682632; surface-modified by aminopropyltriethoxy silane and octadecylamine, Sigma-Aldrich, USA), and exfoliated graphite nanoplatelet (xGnP, C750, XG Sciences, USA), were used as additives.

2.2. Preparation of NM-reinforced A-PA6/WCF composites

Anionic ring-opening polymerization is sensitive to moisture [11,12,44], and thus, every experiment was performed in a moisture-free environment of a glove box. First, the catalyst and activator were put separately into two closed tanks A and B. Then, the CPL and NMs were put, half each, into the two containers. Next, the containers were placed on a heating device and dispersed for 20 min above the melting point of CPL (69 °C) using a magnetic stirrer and a homogenizer. When the temperature reached 10 °C lower than the mold temperature, which was set equal to the polymerization temperature, the mixtures in tanks A (CPL/NM/catalyst) and B (CPL/NM/activator) were mixed for 3 s, and the resulting mixture was injected into the mold cavity containing 9 plies of WCF at a vacuum pressure of 75 kPa. The surface treatment of the WCF was processed using an atmospheric plasma system (API, Korea) with a nozzle height of 11 mm and x-axis nozzle speed of 20 m/min before placing the WCF in the mold. Schematics of the T-RTM and plasma treatment processes are presented in Fig. 1.

2.3. Optimization of polymerization conditions based on polymerization induction time

The cavity size of the mold was 300 × 120 × 2.5 mm (length × width × thickness), and the mold had two resin inlets and outlets. In this cavity, 9-ply WCF was laminated, and the minimum necessary time for producing composites was determined. The process requires at least 3–5 s for mixing, 5–10 s for resin infusion, and 5 s of spare time. Thus, it was confirmed that an approximate total 20–25 s was required as a minimum induction time. In other words, if the reaction accelerates before 20 s and the resin viscosity exceeds 1 Pa s, the solidification is completed during the impregnation of the resin into fibers, such that a proper specimen cannot be obtained. However, if the reaction proceeds beyond 25 s, it does not fulfil the purpose of productivity improvement. For these reasons, the polymerization temperature, catalyst and activator content with induction time of 20–25 s were optimized for each specimen.

2.4. Evaluation for dispersion stability of NM-dispersed CPL

The NM-dispersed CPL was dissolved in diethyl ether (99%, E0697, SAMCHUN Chemical, Korea), and then a Turbiscan (Turbiscan Lab Expert, Formulaction Inc., USA), was used to rapidly evaluate the dispersion stability by an optical measurement method using multiple light scattering [45–47]. It can analyze both particle migration phenomena such as sedimentation and creaming, and particle size variation phenomena such as flocculation and coalescence. Hence, a qualitative evaluation is possible. In this study, each specimen was measured at intervals of 5 min at 50 °C for 1 h, and then the dispersion stability of the samples was compared by quantitative evaluation of the Turbiscan stability index (TSI).

2.5. NM/A-PA6/WCF composite characterization

The degree of monomer conversion (M_c) of the A-PA6 reinforced with NMs was determined by two methods, extraction and evaporation techniques [5,13,48]. The residual CPL after polymerization was extracted from the synthesized A-PA6 using soxhlet extractor with methanol and deionized water for 10 h each. After drying in a vacuum oven at 90 °C overnight, the monomer conversion was calculated by comparing sample weight before and after extraction. The other technique for measuring the monomer conversion was to weigh the sample before and after heating in the furnace up to 230 °C. Because the boiling point of CPL is below the T_m of PA6, the residual CPL is evaporated when temperature reaches 220 °C. Hence, the A-PA6 after heating was expected to be free of CPL. Therefore, the final degree of conversion for both techniques was determined by the following equation.

$$Mc = \frac{Sample\ weight\ after\ removing\ residual\ monomer}{Sample\ weight\ before\ removing\ residual\ monomer} \times 100\% \quad (1)$$

The crystallization temperature, nucleation temperature, melting temperature, and percent crystallinity were measured using differential scanning calorimetry (DSC, TA Instruments Q800, USA). The DSC analysis was performed under a nitrogen atmosphere, over a wide temperature range from −10 to 250 °C with a heating rate of 10 °C/min. The percent crystallinity (X_c) of the A-PA6 was determined using the endothermic peak of the DSC thermogram by the following equation.

$$X_c = (\Delta H_{m,esperiment}/H_{o,literature}) \times 100\% \quad (2)$$

This is the ratio of the melting heat enthalpy of the measured sample (ΔH_m, experiment) and 100% crystalline PA6 (ΔH_o, literature = 230 J/g) [8,38,49].

For measuring the composition change of the plasma-treated WCF surface, X-ray photoelectron spectroscopy (XPS, K-Alpha, Thermo Fisher Scientific, USA) was used in this study. High-resolution spectra such as O1s, C1s, and N1s were observed. To analyze the polar functional groups in detail, the C1s scan was deconvoluted into five Gaussian peaks using a fitting software. Atmospheric plasma treatment typically makes the fiber surface hydrophilic, and hence a contact angle detector (Phoenix 300, SEO, Korea) was employed to evaluate the hydrophilicity of the WCF surface after plasma treatment.

To determine the total production cycle time, the required time for the manufacturing process of the NM/A-PA6/WCF composite was measured by dividing it into four parts: mixing time, resin infusion time, induction time, and solidification time. The sum of these times was taken as the production cycle time, and the demolding time was excluded from the measurement.

The in-plane shear strength, tensile, and flexural properties were determined using a universal testing machine (UTM, 5982, Instron, USA), and both the specimen information and test method were obtained from ASTM D3518, D638 and D790 standards. A crosshead speed of 0.9 mm/min was constantly applied to pull the tensile test samples, which had a 0–90° fiber weaving direction. The testing condition of the in-plane shear strength was same as the tensile test, but the specimens had a different weaving direction (± 45° laminate). The shear strength was determined using the following equation.

$$\tau_{12}^{m} = \frac{P^{m}}{2A} \quad (3)$$

where P^m is the maximum in-plane load, τ_{12}^m is the in-plane shear strength, and A is the cross-sectional area of specimen. In the flexural

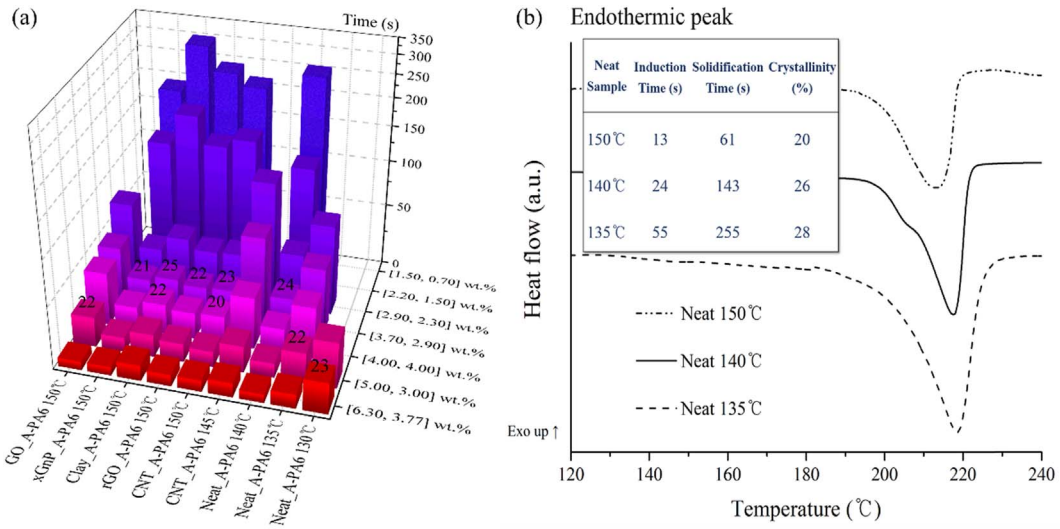

Fig. 2. Optimization of polymerization conditions based on polymerization induction time (a); degree of crystallinity and polymerization time of neat A-PA6 at various processing temperature (b).

test, the crosshead displacement rate of 1 mm/min was applied to push the center of the flexural specimens consistently, and the flexural modulus and strength were evaluated.

3. Results and discussion

3.1. Optimization of polymerization conditions based on polymerization induction time

The polymerization temperature, catalyst-activator contents with 20–25 s polymerization induction time, were optimized for each specimen, and the results are shown in Fig. 2-(a). Several studies on anionic polymerization have shown that the reaction generally takes place between 130 and 160 °C, and higher temperature leads to faster reaction and lower crystallinity. Hence, in this study, the preparation of neat A-PA6 was carried out in the range of 130–150 °C by varying the concentration of the catalyst and activator and by referring to the optimized values obtained from the literature [10,13,50–52]. As can be seen from the results, the induction time for neat A-PA6 decreased with increasing temperature. At 130 °C, the reaction was initiated only with a high amount of catalyst (5–6.3 wt.%) and activator (3–3.77 wt.%), and no reaction occurred with other concentrations. Moreover, the reaction did not occur under the two lowest contents of catalyst and activator at 135 °C. Above 140 °C, the reaction took place at all conditions, but the deviation of the induction time was large depending on the catalyst-activator contents. At even higher temperatures, the induction time of most conditions was within 20 s, owing to the excessively rapid reaction. The measurement results of the crystallinity, induction time, and solidification time at 3.7 wt.% catalyst and 2.9 wt.% activator are shown in Fig. 2-(b). As a result, the higher the polymerization temperature, the higher the polymerization rate, leading to shorter polymerization induction and solidification times. However, crystallinity was greatly reduced because polymerization was completed before crystallization was sufficiently progressed. Additionally, too high a polymerization rate was unsuitable for our experimental setup or for producing large parts. Although crystallinity was high at low temperatures, the polymerization induction and solidification times increased dramatically, considerably reducing the productivity. Therefore, for the fabrication of neat A-PA6, the most appropriate conditions were a catalyst content of 3.7 wt.%, activator content of 2.9 wt.%, and processing temperature of 140 °C.

In the case of specimens containing 0.1 wt.% NMs, the induction time was increased, with the result that suitable induction time was not obtained in the range of 140–145 °C, except when high concentrations of catalyst and activator were used. In addition, the use of large amounts of catalyst and activator is generally inappropriate, because it causes reductions in the molecular weight, toughness, and melting temperature of A-PA6 [6,53]. Thus, the appropriate induction time (20–25 s) was achieved by increasing the temperature to 150 °C with same catalyst and activator content as neat A-PA6. In the case of GO-reinforced A-PA6, the temperature had to be increased above 155 °C to meet the condition, and therefore the catalyst content was slightly increased as an alternative.

Increasing the polymerization temperature reduced the solidification time, although it deteriorated the crystallization properties. However, using the NMs in anionic polymerization was anticipated to greatly reduce the solidification time without loss of crystallinity, owing to their excellent properties as a nucleation agent [22,24,33,54]. Thus, NM-reinforced A-PA6s, prepared at 150 °C, were characterized.

3.2. Dispersion stability of NMs

A combination of a backscattering and transmission sensor with a vertical scanner enables the detection physical heterogeneities over the whole sample height with a vertical resolution up to 20 μm. Therefore, nascent destabilization phenomena by variations of the particle size or local variations of the volume fraction were detected, and then dispersibility was investigated. Most NMs had a black color, with the exception of nanoclay, leading to light absorption, and thus the dispersion stability was evaluated by change in the transmission profile with respect to the backscattering profile. The variation in transmission levels was measured by distinguishing the sample bottle into three sections: top, middle, and bottom. These results are shown in Fig. 3 in terms of the mean value of transmission intensity over time. The transmission level of all samples increases at the top section, owing to a decrease in the concentration of nanoparticles, whereas it has a low level at the bottom section owing to an increase in nanoparticle concentration as part of sediment formation. In particular, in the CNT-dispersed CPL case, a very sharp increase rate is detected before 5 min. This indicates a fast sedimentation rate. The middle section also shows a similar tendency to the top section, but a sharp slope of the CNT sample is found between 5 and 10 min, after which the transmission intensity becomes idle. This means that the sedimentation in the top section is almost complete within 5 min and the sedimentation in the middle section is almost complete within 5–10 min. Conversely, the transmission level at an initial measurement of the CNT sample in the bottom section is very

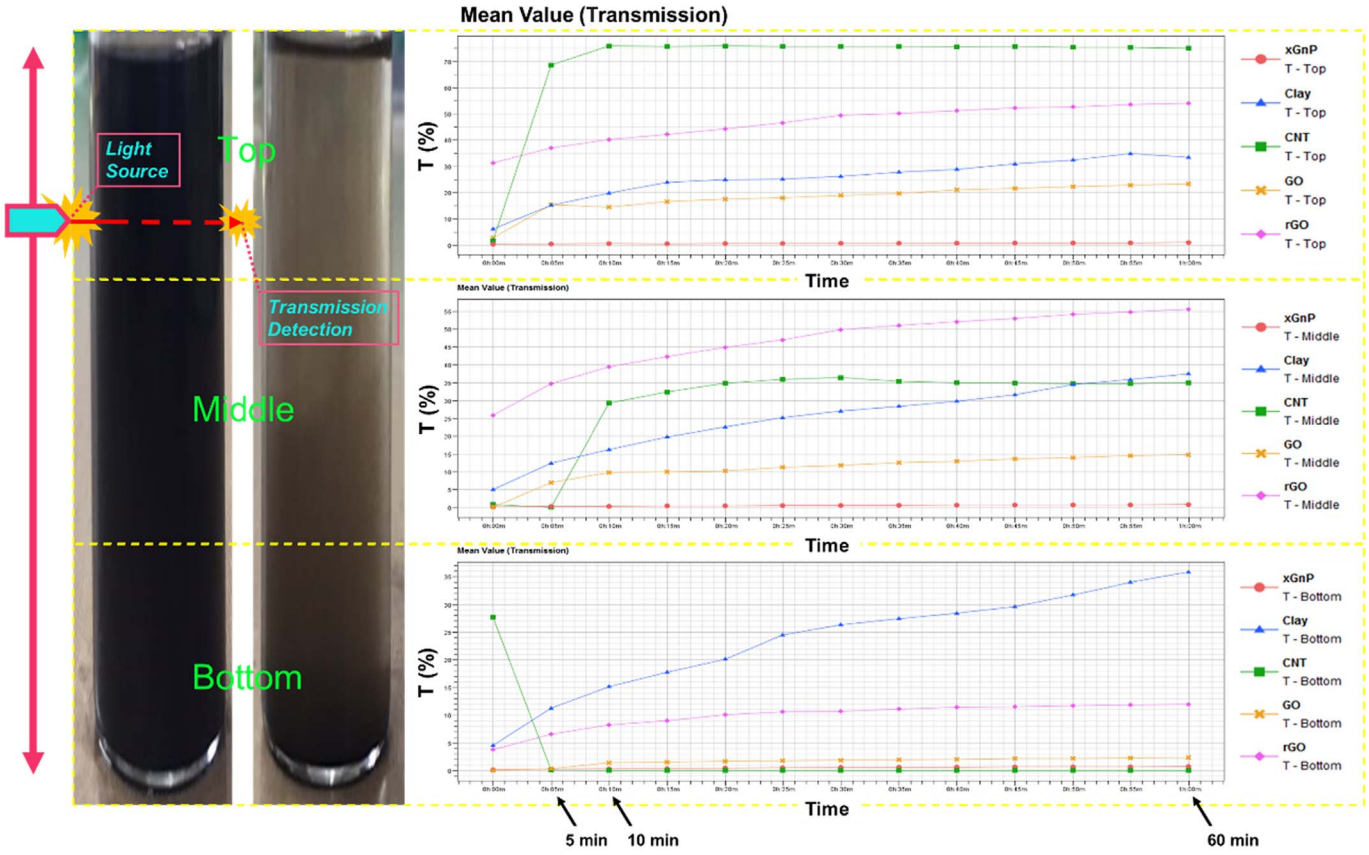

Fig. 3. The variation of transmission levels at top, middle, and bottom section of a cylindrical vial containing various NMs.

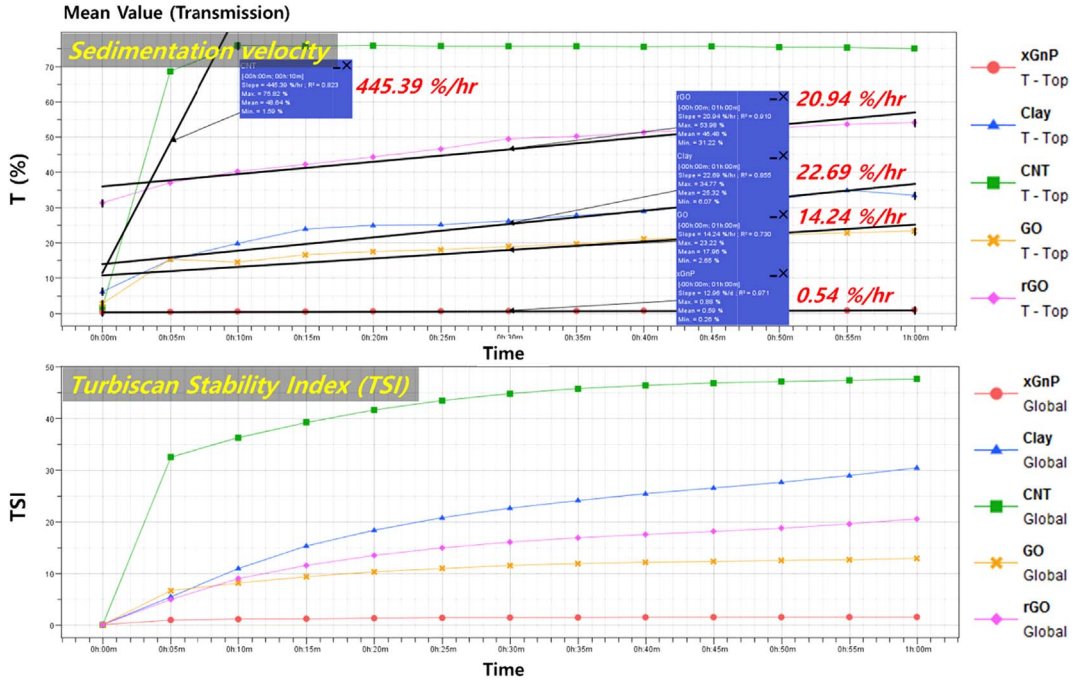

Fig. 4. Sedimentation velocity and Turbiscan Stability Indices (TSI) of NMs.

high compared with other NMs, owing to the creaming phenomenon, but it plunges within 5 min by accelerated sedimentation. These phenomena are representative of the degradation of dispersion stability, indicating that the CNT has poor dispersibility. In the case of nanoclay, the final transmission levels in all sections are similar, because the particle size variation phenomena such as flocculation are more dominant than the particle migration phenomena. The flocculation is also a factor decreasing dispersion stability. The slope of the graph of the top section indicates the sedimentation rate as mentioned above, and the calculated results are presented in Fig. 4. The unit is

Table 1
Monomer conversion (%) of NM-reinforced A-PA6.

Sample	Monomer conversion (%) (extraction)	Monomer conversion (%) (evaporation)
Neat A-PA6	97.90	96.02
CNT/A-PA6	97.94	94.61
rGO/A-PA6	98.25	96.21
Clay/A-PA6	98.61	96.81
GO/A-PA6	98.59	97.01
xGnP/A-PA6	98.52	96.74

transmission level (%) per hour, and the sedimentation rate of the CNTs is even faster than other NMs; in particular, it is approximately 900 times faster than the xGnPs. Hence, if the CNTs are used as an additive to the T-RTM process, a pretreatment process such as oxidation for improving dispersibility is considered to be necessary. The other sedimentation rates decrease in the order of nanoclay, rGO, GO, and xGnP. In particular, the xGnP-dispersed sample has the best dispersion stability, because it has low transmission variation in all sections and the lowest rate of sedimentation. For a more accurate and comprehensive comparison, the TSI, a quantitative analysis provided by Formulaction Inc., is indicated in Fig. 4. The TSI is typically useful to distinguish, compare, and evaluate the dispersion stability between different samples, and a lower TSI value indicates better dispersion stability. The results show that, as expected, the xGnPs have the best dispersion stability, whereas the CNTs have the worst dispersion stability. In the case of other NMs, it was difficult to judge which NM is more stable, but by using the TSI, it is quantitatively confirmed that dispersion stability is better in the order of GO, rGO and nanoclay.

3.3. Monomer conversion

The monomer conversion of A-PA6 was increased by adding the NMs at the extraction method, but the conversion of the CNT-reinforced A-PA6 sample was lower than neat A-PA6 at the evaporation method, as shown in Table 1. According to Nylon Plastics Handbook, edited by Melvin I. Kohan [55], increasing the polymerization temperature reduced the degree of crystallinity because the thermal motion of the

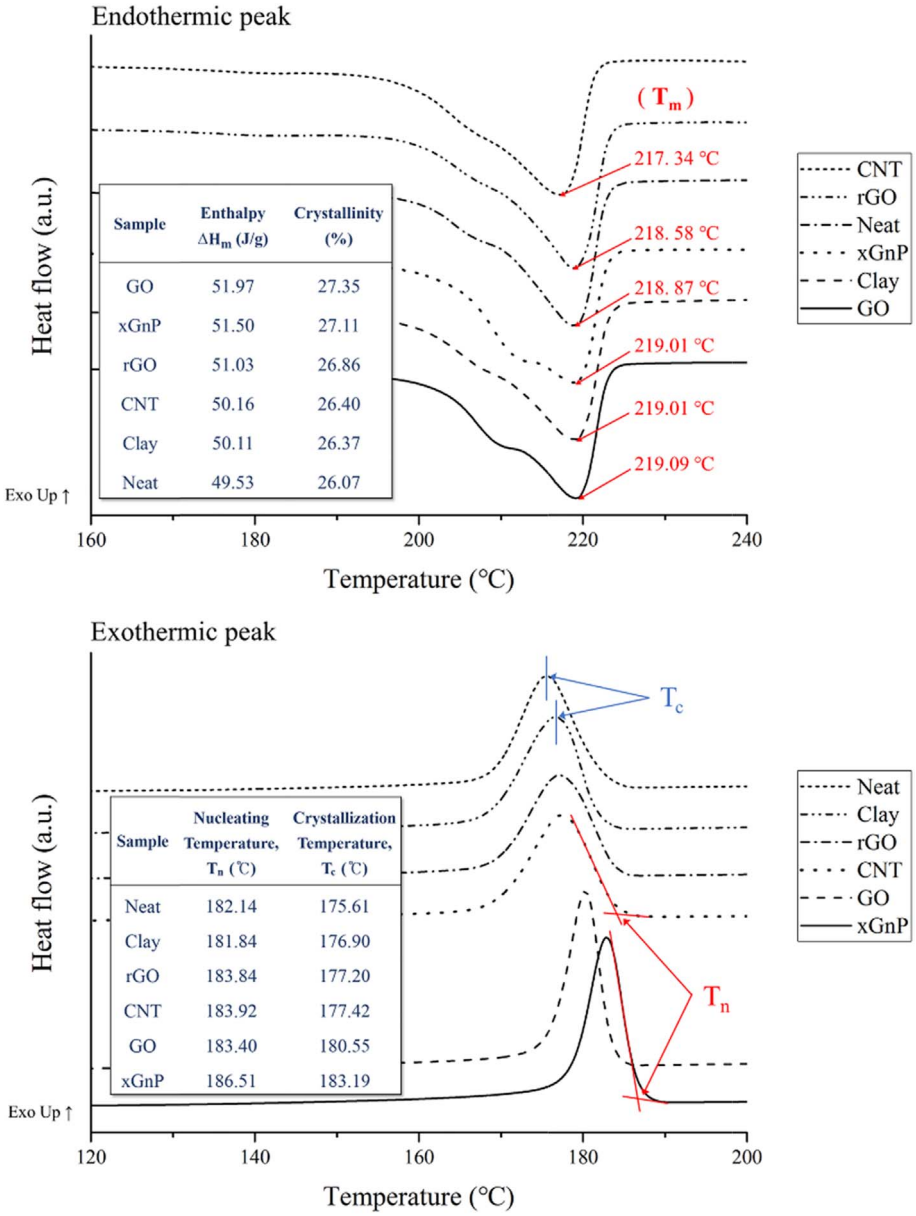

Fig. 5. Endothermic and exothermic peaks of DSC thermogram, and crystallization behavior upon NM-reinforced A-PA6.

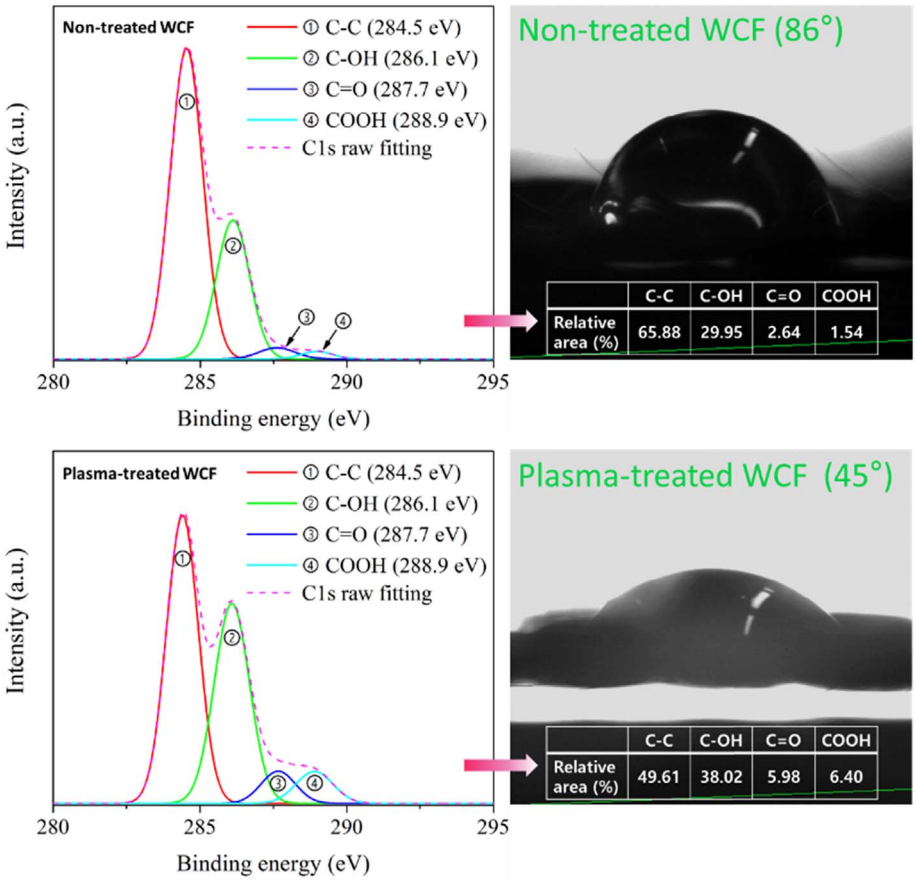

Fig. 6. XPS C1s-deconvoluted peaks (left) and contact angle (right) of WCF surface before and after plasma treatment.

Table 2
Mean value of each process time and overall manufacturing process cycle time (in seconds).

Sample	Mixing time	Resin infusion time (Non-treated)	Resin infusion time (Plasma-treated)	Polymerization induction time	Solidification time	Process cycle time
Neat A-PA6/WCF	3	4.03	3.52	24	143	173.52
CNT/A-PA6/WCF	3	4.78	4.52	23	69	99.52
rGO/A-PA6/WCF	3	4.64	4.23	22	67	96.23
Clay/A-PA6/WCF	3	4.23	3.63	25	81	112.63
GO/A-PA6/WCF	3	4.35	3.98	21	46	73.98
xGnP/A-PA6/WCF	3	4.19	3.71	22	50	78.71

polymer chains became too high to let them crystallize, which resulted in a decrease in the monomer conversion. In this study, although the polymerization temperature of NM-reinforced A-PA6 was 10 °C higher than the neat A-PA6, the monomer conversion of NM-reinforced samples was higher than the neat sample, owing to the nucleating role of NMs, which will be discussed in the next section. Another reason, the slow solidification (polymerization) rate of neat A-PA6, can be also considered because active groups in the monomer can be buried inside a growing crystal before they can polymerize by high crystallization rate at 140 °C [5,11]. For these reasons, most NM-reinforced A-PA6 samples had a higher conversion, but the CNT-reinforced sample had similar or lower conversion as compared with neat A-PA6. This is due to the poor dispersion stability, leading to an increase in amorphous phase by preventing the diffusion of CPL.

3.4. Crystallization behavior

The DSC thermograms are presented in Fig. 5. The NMs can stabilize the crystalline sites thereby promoting the rate of the crystallization, and increasing the degree of crystallinity. Thus, all the NM-reinforced A-PA6s have the higher degree of crystallinity than neat A-PA6. From the endothermic peaks, it is confirmed that the melting temperature is shifted to a higher temperature for samples reinforced with xGnP, nanoclay, and GO, whereas in CNT- and rGO-reinforced samples, the melting point decreases slightly as compared with the neat sample. This is due to the low dispersion stability and high volume fraction, which can make nanoparticles agglomerated together easily, leading to a reduction the interfacial area of the NMs available for nucleation. The exothermic peak shows that the addition of the NMs increases the nucleation temperature and crystallization temperatures of the A-PA6; particularly, the GO- and xGnP-reinforced A-PA6 samples have the highest nucleation and crystallization temperatures, as well as narrow and high peak shapes. It means that they have a much higher rate of crystallization as compared to other samples. Therefore, when the polymerization rate is increased, the crystallization rate is also increased due to the NMs, which allows sufficient crystallization to proceed while polymerization is completed. Consequently, although the NM-reinforced A-PA6s were polymerized at a temperature 10 °C higher

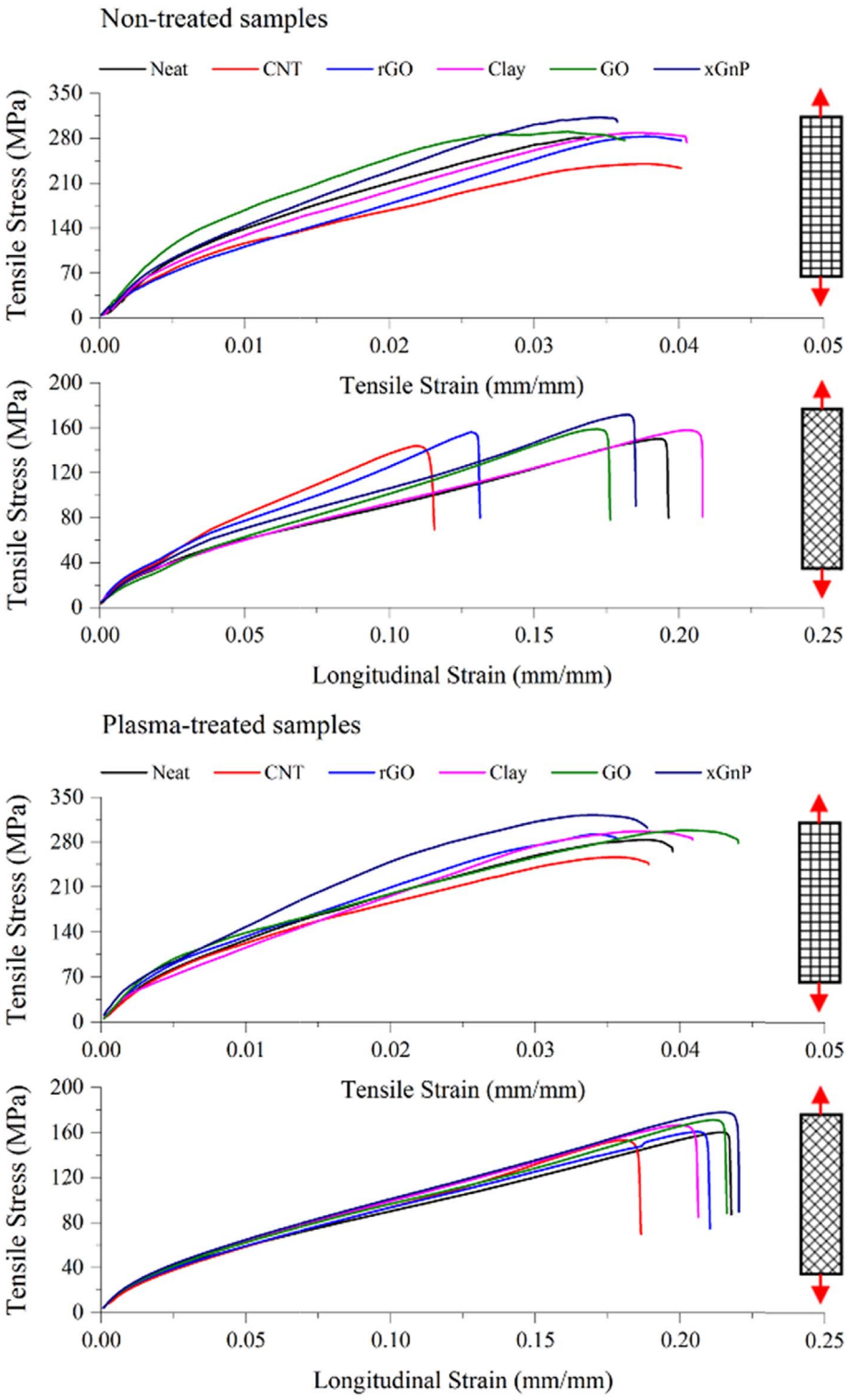

Fig. 7. Stress-strain curves of NM/A-PA6/WCF composite depending on plasma treatment and tensile loading direction of specimen for tensile and in-plane shear responses.

than neat A-PA6, which is one of the main factors decreasing crystallinity, they had higher crystallinity. Both the degree of crystallinity and melting temperature are correlated with monomer conversion. Therefore, the GO-, nanoclay-, and xGnP-reinforced samples exhibit better crystallization properties in common with monomer conversion.

3.5. Surface analysis of atmospheric-plasma-treated WCF

The change in the composition of the WCF surface was analyzed using XPS. Over the entire range of the XPS scan (0–1400 eV), the C1s (280–295 eV), O1s (525–540 eV), N1s (394–410 eV), and Si2p (97–107 eV) peaks were present in all samples in common, and the C1s-deconvoluted peaks comprised C–C (284.5 eV), C–OH (286.1 eV), C = O (287.7 eV), and COOH (288.9 eV) peaks were investigated to confirm an effect of plasma treatment. From the results of the XPS analysis (see Fig. 6), the oxygen functional groups such as hydroxyl, carbonyl, and carboxyl groups considerably increase after plasma treatment. Because these functional groups can make the fiber surface hydrophilic and

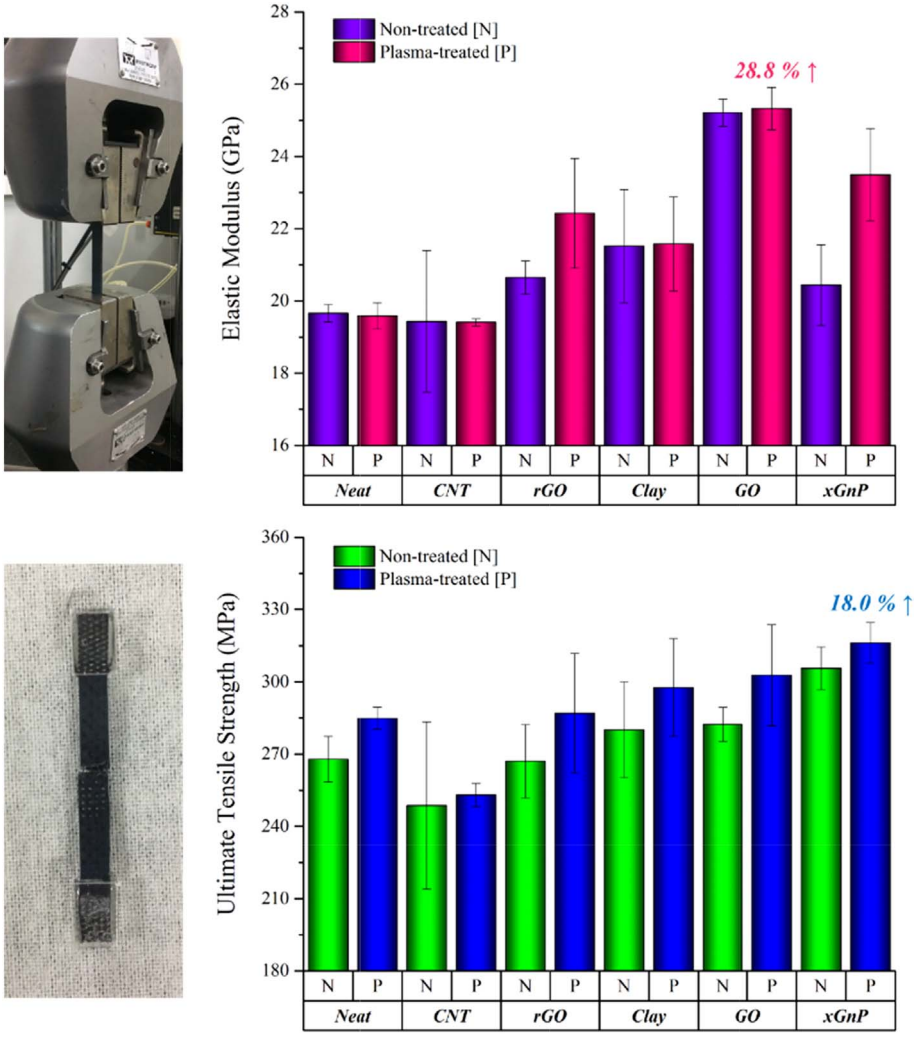

Fig. 8. Tensile properties of NM/A-PA6/WCF composites depending on plasma treatment.

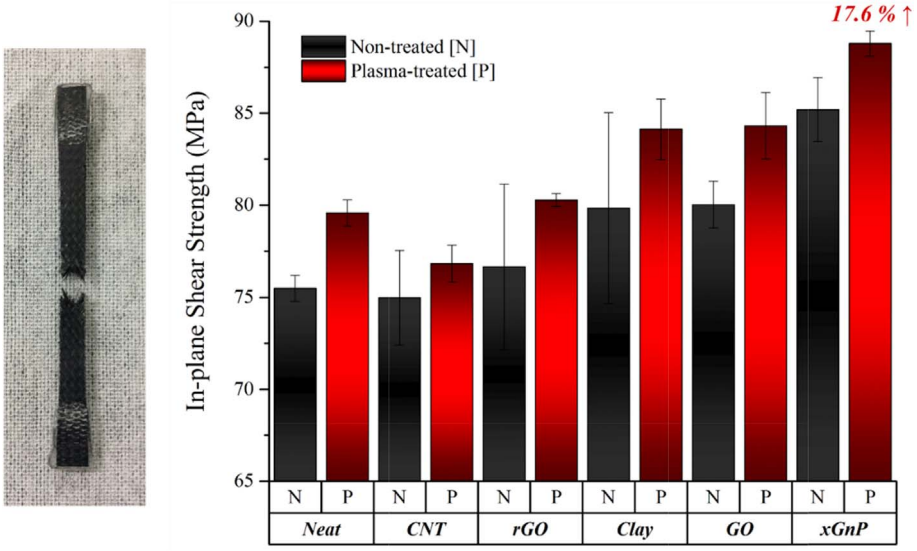

Fig. 9. In-plane shear strength of NM/A-PA6/WCF composites depending on plasma treatment.

react with A-PA6 and NMs to form hydrogen bonding, the increase in the functional groups through the atmospheric plasma treatment promotes the resin impregnation rate into the fibers and improves the interfacial adhesion between the fibers and resin [19–21]. Moreover, the result of the water contact angle measurement presented in Fig. 6 also confirms that the plasma treatment positively affects the fiber

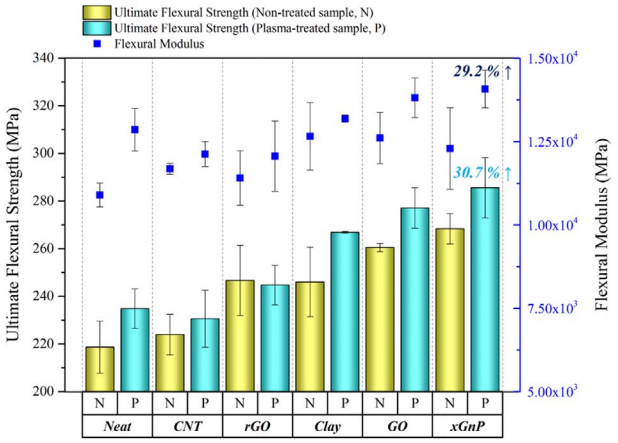

Fig. 10. Flexural properties of NM/A-PA6/WCF composites depending on plasma treatment.

surface area and the changes in surface composition, thereby reducing the contact angle.

3.6. Process cycle time of the T-RTM

As described in Section 2.5, the manufacturing time was measured by dividing the process into four parts (mixing, infusion, polymerization induction, and solidification), and the results are shown in the Table 2. The mixing time was always fixed at 3 s, and the induction time was already measured during the optimization described in Section 3.1. Therefore, we will focus here on the resin infusion time and solidification time. As anticipated, the resin infusion time into the mold, where the nine plies of WCF are laminated, is the shortest for neat CPL. However, the CPL dispersed with NMs with the higher volume fraction and lower dispersion stability (e.g., CNT, rGO) at the same wt.% increases resin infusion time. Moreover, plasma-treated fibers reduce the resin infusion time slightly, because the polar functional groups on the fiber surface increase the resin impregnation rate into fibers. Due to the small space of the mold cavity, the time gap was not very noticeable, except for the CNT and rGO samples. The ratio of the resin infusion time to the total process cycle time is very low, but it is expected that the effect of reducing the resin infusion time through plasma treatment can be clearly obtained at large-sized products. As for the solidification time, which accounts for the largest portion of the total processing time, the time gap between A-PA6/WCF and NM/A-PA6/WCF composites is very large because not only the polymerization temperature of the NM/A-PA6/WCF composite is higher than the A-PA6/WCF composite, but also the NMs accelerate the reaction by increasing the crystallization rate. In particular, the GO-reinforced composite has the shortest solidification time, because the slightly higher catalyst content is used to achieve the proper induction time. The xGnP-reinforced composite with the highest dispersion stability and crystallization rate has the second shortest solidification time. In conclusion, the total process cycle time of the NM/A-PA6/plasma-treated WCF composite decreases by more than two times (235%) compared to the neat A-PA6/WCF composite, without loss of crystallinity.

3.7. Mechanical properties of the NM/A-PA6/WCF composites

Twelve kinds of specimens depending on NMs and plasma treatment were tested to investigate the tensile, in-plane shear, and flexural properties. From the results of the tensile tests (see Figs. 7 and 8), the CNT-reinforced specimen with poor dispersion stability shows slight decreases in elastic modulus and tensile strength compared to the neat specimen, owing to agglomerated CNT particles caused by van der Waals attractive force and entanglement at high temperature; this leads to a reduction in the interfacial bonding between the fiber surface and resin. The highest elastic modulus and ultimate tensile strength are shown in the specimens reinforced with GO and xGnP, respectively, increasing by 28.8 and 18.0%, respectively, compared to the A-PA6/WCF specimen. In addition, the test results show that the plasma treatment not only reduces resin infusion time but also increases the mechanical properties. After plasma treatment, the elastic modulus and strength increased by 4.1 and 5.4% on average, respectively.

The in-plane shear strength results (see Fig. 9) show that the shear strength is increased in the NM/A-PA6/WCF specimens, excluding the CNT-reinforced specimen. Moreover, in S–S curves before and after the plasma treatment (Fig. 7), the fracture of the composites made by surface-treated fibers occurs later than for the non-treated specimens. This is because the polar functional groups such as hydroxyl, carbonyl, and carboxyl increased on the fiber surface, leading to increased interfacial bonding properties. Hence, after plasma treatment, in-plane shear strength increased by 4.4% on average.

The three-point bending test results show that the flexural properties of the NM-reinforced composite are proportional to the crystallization properties and the dispersion stability. In Fig. 10, the maximum flexural modulus and flexural strength are increased by 29.2 and 30.7%, respectively, for the xGnP-reinforced A-PA6/plasma-treated WCF composite as compared to the A-PA6/WCF composite. This is somewhat different from the results of the previous tensile test, in which the xGnP-reinforced specimen had no highest modulus. Before the plasma treatment, the xGnP-reinforced A-PA6/WCF composite has relatively high flexural modulus, which is consistent with the other test results, but it has the highest value after plasma treatment. This implies that the improvement in interfacial bonding between the resin and fiber by plasma treatment is even more effective for the xGnP-reinforced A-PA6/WCF composite as compared with the other NM-reinforced composites, because xGnPs shows the best dispersion stability in resin. Generally, the flexural properties of fiber-reinforced composites are more influenced by the polymer matrix and interfacial boding properties than the intrinsic fiber properties. Therefore, the average improvement rate of the flexural modulus (10.2%) and strength (5.2%) by the plasma treatment is higher than for the other test results. The GO- and xGnP-reinforced A-PA6/plasma-treated WCF composites not only showed the best mechanical properties, but also provided the shortest process cycle time. Thus, the GO and xGnP are the most suitable nano-additives for the T-RTM process using PA6.

4. Conclusions

Polymerization and crystallization occurred simultaneously during the anionic ring-opening polymerization of CPL in the mold, causing a rapid reaction and yielding composites with excellent mechanical properties. Higher polymerization temperature results in a faster production rate, however, this might not lead to polymers with a high crystallinity and good mechanical properties. Thus, a compromise between productivity and good mechanical properties is inevitable. To overcome these limitations, the NMs were used as a reinforcing agent, allowing the polymerization to take place at a higher temperature by delaying the induction time. This not only dramatically reduced the solidification time but also increased the mechanical properties by preventing the decrease in crystallinity owing to the role of the NMs as a great nucleation agent. Moreover, by using the fibers treated by atmospheric plasma, the resin transfer rate in the mold was increased, which contributed to shortening the overall process cycle time. Additionally, the mechanical properties were improved by increasing the polar functional groups on the fiber surface. In conclusion, when NMs and plasma treatment are applied to the T-RTM process simultaneously, not only was the process cycle time reduced by a factor of more than two (235%), the mechanical properties were also enhanced.

Acknowledgments

This work was supported by the National Research Foundation of Korea grant funded by the Ministry of Science and ICT (NRF-2017R1A5A1015311) and the Economic Collaborative Industry Development Program through the Korea Evaluation Institute of Industrial Technology funded by the Ministry of Trade, Industry and Energy (Grant No. R0003923) of Korea.

References

[1] Choi CH, LEE GG, Choi C, Kim HJ, Kil YK, Yoon YH, et al. Battery pack case assembly for electric and hybrid vehicles using a plastic composite and method for manufacturing the same. Patents; 2014.
[2] Dogan A, Arikan V. Low-velocity impact response of E-glass reinforced thermoset and thermoplastic based sandwich composites. Compos B Eng 2017;127:63–9.
[3] Stewart R. Thermoplastic composites — recyclable and fast to process. Reinforc Plast 2011;55(3):22–8.
[4] Bitterlich MEM, Wollny A, Desbois P, Renkl J, Schmidhuber S. Thermoplastic resin transfer molding (T-RTM): tailored to reactive polyamide 6. Kunstst Int 2014;03:47–51.
[5] van Rijswijk K, Bersee HEN, Beukers A, Picken SJ, van Geenen AA. Optimisation of anionic polyamide-6 for vacuum infusion of thermoplastic composites: influence of polymerisation temperature on matrix properties. Polym Test 2006;25(3):392–404.
[6] van Rijswijk K, Bersee HEN, Jager WF, Picken SJ. Optimisation of anionic polyamide-6 for vacuum infusion of thermoplastic composites: choice of activator and initiator. Compos Part a-Appl S 2006;37(6):949–56.
[7] van Rijswijk K, Bersee HEN. Reactive processing of textile fiber-reinforced thermoplastic composites - an overview. Compos Part a-Appl S 2007;38(3):666–81.
[8] Xu S, Ye L. Monomer casting nylon-6-b-polyether amine copolymers: synthesis and properties. Compos B Eng 2015;79:170–81.
[9] Khodabakhshi K, Gilbert M, Dickens P, Hague R. Optimizing conditions for anionic polymerization of caprolactam for inkjetting. Adv Polym Technol 2010;29(4):226–36.
[10] Berg LF. Process development for the reactive injection moulding of caprolactam intermediates. Institute for Applied Materials Science and Engineering, Karlsruhe Institute of Technology; 2011.
[11] Khodabakhshi K. Anionic polymerisation of caprolactam: an approach to optimising thr polymerisation condition to be used in the jetting process. UK: Loughborough University; 2011.
[12] Hsieh H, Quirk RP. Anionic polymerization: principles and practical applications. Taylor & Francis; 1996.
[13] Barhoumi N, Maazouz A, Jaziri M, Abdelhedi R. Polyamide from lactams by reactive rotational molding via anionic ring-opening polymerization: optimization of processing parameters. Express Polym Lett 2013;7(1):76–87.
[14] Khodabakhshi K, Gilbert M, Fathi S, Dickens P. Anionic polymerisation of caprolactam at the small-scale via DSC investigations. J Therm Anal Calorim 2014;115(1):383–91.
[15] Scalici T, Fiore V, Valenza A. Effect of plasma treatment on the properties of Arundo Donax L. leaf fibres and its bio-based epoxy composites: a preliminary study. Compos B Eng 2016;94:167–75.
[16] Ren GN, Zhang ZZ, Zhu XT, Men XH, Jiang W, Liu WM. Combined effect of air-plasma treatment and lubricant filling on the dry sliding wear behavior of hybrid PTFE/Nomex fabric/phenolic composite. Compos Sci Technol 2014;100:204–11.
[17] Dilsiz N. Plasma surface modification of carbon fibers: a review. J Adhes Sci Technol 2000;14(7):975–87.
[18] Tiwari S, Bijwe J. Surface treatment of carbon fibers - a review. Procedia Technol 2014;14(Supplement C):505–12.
[19] Li J, Zhou Z. The TPB properties of plasma-treated carbon fiber-reinforced polystyrene composites. Polym Plast Technol Eng 2009;49(1):20–3.
[20] Park SJ, Lee EJ, Kim BJ. A study of atmospheric-pressure CHF3/Ar plasma treatment on dielectric characteristics of polyimide films. J Colloid Interface Sci 2008;319(1):365–9.
[21] Park SJCY, Moon CW, Suh DH, Im SS, Kim YC. A study of atmospheric plasma treatment on surface energetics of carbon fibers. Bull Kor Chem Soc 2010;31(2):335–8.
[22] Razavi-Nouri M, Ghorbanzadeh-Ahangari M, Fereidoon A, Jahanshahi M. Effect of carbon nanotubes content on crystallization kinetics and morphology of polypropylene. Polym Test 2009;28(1):46–52.
[23] Kobayashi S, Kitagawa J. Effect of fine particle incorporation into matrix on mechanical properties of plain woven carbon fiber reinforced plastics fabricated with vacuum assisted resin transfer molding. Compos B Eng 2016;85:31–40.
[24] Assouline E, Lustiger A, Barber AH, Cooper CA, Klein E, Wachtel E, et al. Nucleation ability of multiwall carbon nanotubes in polypropylene composites. J Polym Sci Pol Phys 2003;41(5):520–7.
[25] Bagotia N, Choudhary V, Sharma DK. Studies on toughened polycarbonate/multiwalled carbon nanotubes nanocomposites. Compos B Eng 2017;124:101–10.
[26] Madaleno L, Schjodt-Thomsen J, Pinto JC. Morphology, thermal and mechanical properties of PVC/MMT nanocomposites prepared by solution blending and solution blending plus melt compounding. Compos Sci Technol 2010;70(5):804–14.
[27] Du SS, Li F, Xiao HM, Li YQ, Hu N, Fu SY. Tensile and flexural properties of graphene oxide coated-short glass fiber reinforced polyethersulfone composites. Compos B Eng 2016;99:407–15.
[28] Wang H, Xie GY, Fang MH, Ying Z, Tong Y, Zeng Y. Mechanical reinforcement of graphene/poly(vinyl chloride) composites prepared by combining the in-situ suspension polymerization and melt-mixing methods. Compos B Eng 2017;113:278–84.
[29] Sanchez-Jimenez PE, Perez-Maqueda LA, Perejon A, Criado JM. Nanoclay nucleation effect in the thermal stabilization of a polymer nanocomposite: a kinetic mechanism change. J Phys Chem C 2012;116(21):11797–807.
[30] Lv Q, Wu D, Qiu Y, Chen J, Yao X, Ding K, et al. Crystallization of Poly(ε-caprolactone) composites with graphite nanoplatelets: relations between nucleation and platelet thickness. Thermochim Acta 2015;612(Supplement C):25–33.
[31] Li L, Li B, Hood MA, Li CY. Carbon nanotube induced polymer crystallization: the formation of nanohybrid shish–kebabs. Polymer 2009;50(4):953–65.
[32] Yang S, Li Y, Liang YY, Wang WJ, Luo Y, Xu JZ, et al. Graphene oxide induced isotactic polypropylene crystallization: role of structural reduction. RSC Adv 2016;6(28):23930–41.
[33] Fairgrieve S. Nucleating agents. Rapra Technology Limited; 2007.
[34] Tao Zheng QL, Qian Zhou, Huayi Li, Qian Xing, Liaoyun Zhang, Youliang Hu. Expected nucleation effects of carboxylic acid salts on poly(1-butene). Polyolefins J 2015;3(1):37–45.
[35] Marco C, Gomez MA, Ellis G, Arribas JM. Highly efficient nucleating additive for isotactic polypropylene studied by differential scanning calorimetry. J Appl Polym Sci 2002;84(9):1669–79.
[36] Simanke AG, de Azeredo AP, de Lemos C, Mauler RS. Influence of nucleating agent on the crystallization kinetics and morphology of polypropylene. Polimeros 2016;26(2):152–60.
[37] Faghihi M, Shojaei A, Bagheri R. Characterization of polyamide 6/carbon nanotube composites prepared by melt mixing-effect of matrix molecular weight and structure. Compos B Eng 2015;78:50–64.
[38] Hwang SH, Kim BJ, Baek JB, Shin HS, Bae IJ, Lee SY, et al. Effects of process parameters and surface treatments of graphene nanoplatelets on the crystallinity and thermomechanical properties of polyamide 6 composite fibers. Compos B Eng 2016;100:220–7.
[39] Liang JZ, Du Q, Tsui GCP, Tang CY. Tensile properties of graphene nano-platelets reinforced polypropylene composites. Compos B Eng 2016;95:166–71.
[40] Lv ZP, Yang YF, Wu R, Tong YC. Design and properties of a novel nucleating agent for isotactic polypropylene. Mater Des 2012;37:73–8.
[41] Zhu ZC, Shi SJ, Wang HL. Radical chain polymerization catalyzed by graphene oxide and cooperative hydrogen bonding. Macromol Rapid Commun 2016;37(2):187–94.
[42] Muller AJ, Arnal ML, Trujillo M, Lorenzo AT. Super-nucleation in nanocomposites and confinement effects on the crystallizable components within block copolymers, miktoarm star copolymers and nanocomposites. Eur Polym J 2011;47(4):614–29.
[43] Xu XB, Li Q, Xiong CD. Crystallization behavior of poly(p-dioxanone) with cyclodextrin complex and nucleation mechanism discussion. RSC Adv 2016;6(90):87169–78.
[44] Rusu G, Ueda K, Rusu E, Rusu M. Polyamides from lactams by centrifugal molding via anionic ring-opening polymerization. Polymer 2001;42(13):5669–78.
[45] Bru P, Brunel L, Buron H, Cayre I, Ducarre X, Fraux A, et al. Particle size and rapid stability analyses of concentrated dispersions: use of multiple light scattering technique. ACS Sym Ser 2004;881:45–60.
[46] Kim HS, Park WI, Kang M, Jin HJ. Multiple light scattering measurement and stability analysis of aqueous carbon nanotube dispersions. J Phys Chem Solid 2008;69(5–6):1209–12.
[47] Seo DW, Yoon WJ, Park SJ, Jo MC, Kim JS. The preparation of multi-walled CNT–PMMA nanocomposite. Carbon Sci 2006;7(4):266–70.
[48] Zhang CL, Feng LF, Hu GH. Anionic polymerization of lactams: a comparative study on various methods of measuring the conversion of epsilon-caprolactam to polyamide 6. J Appl Polym Sci 2006;101(3):1972–81.
[49] Cartledge HCY, Baillie CA. Studies of microstructural and mechanical properties of nylon/glass composite - Part I - the effect of thermal processing on crystallinity, transcrystallinity and crystal phases. J Mater Sci 1999;34(20):5099–111.
[50] BrüggemannChemical. Technical data sheet. BRUGGOLEN® C10/C 20/C 20 P; 2014.
[51] Kugler A, Eckert A, Laufer W, Witt M, Joachimi D, Margraf G, et al. Novel compositions for producing cast polyamides. Google Patents; 2015.
[52] RheinChemieCoporation. Technical data sheet. Addonyl® Kat NL/8120; 2014.
[53] Fornes TD, Yoon PJ, Keskkula H, Paul DR. Nylon 6 nanocomposites: the effect of matrix molecular weight (vol 42, pg 9929, 2001). Polymer 2002;43(7):2121–2.
[54] Modesti M, Lorenzetti A, Bon D, Besco S. Thermal behaviour of compatibilised polypropylene nanocomposite: effect of processing conditions. Polym Degrad Stabil 2006;91(4):672–80.
[55] Kohan MI, Kohan MI. Nylon plastics handbook. Hanser Publishers; 1995.